Graphene oxide-polyamine pre-programmable nanoreactors with sensing capability for corrosion protection of materials

Kou Yang[1,2], Zhitao Hu[1,2], Xiaolai Li[1,3], Konstantin Nikolaev[1,2], Gan Kai Hong[1,2], Natalia Mamchik[1,2], Ivan Erofeev[4,5], Utkur M. Mirsaidov[5,6], Daniel J. Blackwood[1], Dmitry G. Shchukin[7], Maxim Trushin[1,2], Kostya S. Novoselov[1,2] and Daria V. Andreeva[1,2]*

[1]Department of Materials Science and Engineering, National University of Singapore, 117575, Singapore
[2]Institute for Functional Intelligent Materials, National University of Singapore, 117544, Singapore
[3]National University of Singapore (Suzhou) Research Institute, 215123, Jiangsu, China
[4]Department of Biological Sciences, National University of Singapore, 117558, Singapore
[5]Centre for BioImaging Sciences, National University of Singapore, 117543, Singapore
[6]Department of Physics, National University of Singapore, 117551, Singapore
[7]Stephenson Institute for Renewable Energy, University of Liverpool, L69 7ZF, United Kingdom

Corrosion naturally spoils refined metals by converting them into oxides. The conventional method for preventing corrosion is passivation – the formation of a uniform film acting as a barrier to metal dissolution. However, selective treatment of corrosion sites relevant to multicomponent alloys cannot be achieved by standard passivation techniques. Here, we demonstrate a concept of the nanoreactors, which are able to controllably release or adsorb protons or hydroxides directly on corrosion sites, hence, selectively regulating the corrosion reactions. A single nanoreactor comprises a nanocompartment wrapped around by a pH-sensing membrane represented, respectively, by a halloysite nanotube and a graphene-oxide/polyamine envelope. A nanoreactor response is determined by the change of a signaling pH on a given corrosion site. The nanoreactors are self-assembled and suitable for mass-line production. The concept creates an opportunity for developing smart anticorrosion coatings, which are non-toxic, selective, and inexpensive.

Smart, chemically active nanomaterials are currently a very active area of research, with possible applications ranging from healthcare to catalysis. The basic characteristics of such materials are the ability to monitor the environment and supply/absorb reaction components depending on the reaction pathway and required properties, and possibly even to act as nanoreactors for the chemical processes' regulation. To this end, such active nanomaterials should contain nanocompartments for component storage, as well as the ion diffusion control mechanism equipped with sensor abilities. The best properties and performance of such

nanomaterials can be achieved if we assemble multidimensional composites, which include components of different dimensionalities. Here we propose a novel sustainable eco-friendly anticorrosion multidimensional nanoreactors that are inclusive for the protection of different materials and active corrosion control.

Corrosion is one of the complex natural processes which is accompanied by the uptake and release of ions and local pH change.[1, 2] Typical anticorrosion coating acts as a barrier for corrosive species[3-5] and passivates corrosion using non-eco-friendly corrosion inhibitors.[6] Chromates,[7] nitrites,[8] film-forming acetylenic alcohols,[9] mercapto compounds, and azole derivatives[10] form protective films and recover the damaged areas. However, these chemicals are cancerogenic, they are dangerous water and soil pollutants.[11] As a part of sustainable corrosion control, the global corrosion inhibitor market focuses on the development of novel sustainable approaches. To win the sustainable anticorrosion challenge, the size of the inhibitor market is expected to grow to USD 10.1 billion by 2026.[12] The growing demand for clean and safe corrosion protection accelerates the development of novel sustainable formulations with simultaneous passivation of different corrosion pathways.

The chemistry of corrosion is complex, especially because corroded materials have a complex composition. Aluminum alloy AA2024 is used in this work to demonstrate the capability of our nanoreactors to simultaneously passivate several corrosion pathways and provide total corrosion protection. Red/ox reactions at intermetallic and metal oxidation upon mechanical damage of the oxide layer represent two pathways of aluminum alloys' corrosion[13]. The shift of pH to either acidic or basic values accompanies such reactions[14]. In the case of AA2024, Cu/Fe intermetallic inclusions act as cathodes to drive the corrosion of the Al matrix. The main cathodic reactions are the reduction of dissolved oxygen ($O_2+2H_2O+4e^-\leftrightarrow4OH^-$) and the production of hydrogen ($2H^++2e^-\rightarrow H_2$), which results in an increase in the local pH and the formation of H_2 that could be detrimental to the sol-gel coating (Fig. 1a, right). While at the Al matrix, a drop in pH occurs from the anodic reaction, which involves aluminum dissolution ($2Al\rightarrow2Al^{3+}+3e^-$) and hydrolysis reaction to produce an acidic environment inside the pits ($Al^{\circ}+H_2O\leftrightarrow AlOH^-+H^+ + e^-$) (Fig. 1a, left). Here we propose active anticorrosion nanoreactors that sense the local pH change and release OH^-/H^+ ions to passivate the corrosion reactions.
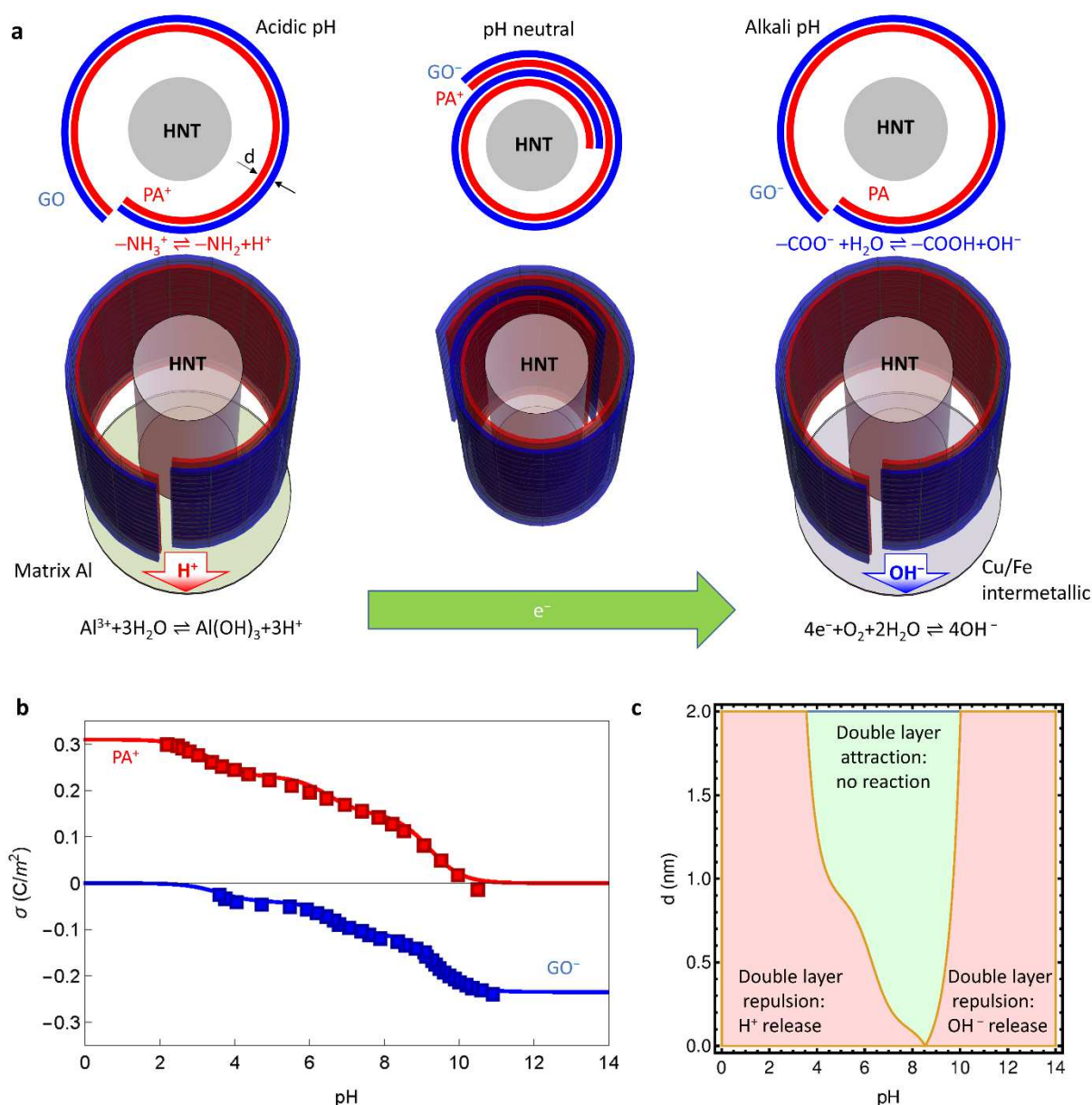
a

Acidic pH HNT GO PA$^+$ d

$-NH_3^+ \rightleftharpoons -NH_2 + H^+$

pH neutral GO$^-$ PA$^+$ HNT

Alkali pH HNT GO$^-$ PA

$-COO^- + H_2O \rightleftharpoons -COOH + OH^-$

HNT Matrix Al H$^+$

$Al^{3+} + 3H_2O \rightleftharpoons Al(OH)_3 + 3H^+$

e$^-$

HNT OH$^-$ Cu/Fe intermetallic

$4e^- + O_2 + 2H_2O \rightleftharpoons 4OH^-$

b

PA$^+$

GO$^-$

σ (C/m^2)

pH

c

Double layer attraction: no reaction

Double layer repulsion: H$^+$ release

Double layer repulsion: OH$^-$ release

d (nm)

pH

Fig. 1 Anticorrosion concept implemented by means of nanoreactors comprising halloysite nanotubes wrapped around by graphene-oxide/polyamine (GO/PA) pH-sensing membranes. a Top and side views of the nanoreactors in pH-neutral (middle), acidic (left) and alkali (right) environments. The nanoreactors deliver excess protons (left) or hydroxides (right) onto the respective corrosion sites and change the corrosion reaction equilibrium in accordance with the Le Chatelier's principle. The interlayer distance *d* is about 1 nm. **b** Surface charge densities for GO and GOPA measured by titration and fitted by the Henderson-Hasselbalch equation with pK$_{a1}$=3.35, pK$_{a2}$=6.5, pK$_{a3}$=9.2 for PA and pK$_{a1}$=2.95, pK$_{a2}$=6.7, pK$_{a3}$=9.4 for GO. The GO and PA layers are strongly charged in alkali and acidic environment, respectively, as indicated in panel (a). **c** The total double-layer electrostatic interaction may result in either interlayer repulsion or attraction depending on pH and interlayer distance. The transition from the interlayer attraction to repulsion corresponds to the activation of the nanoreactor.

To assemble the nanoreactors, we employ halloysite nanotubes[15] (HNTs) as the internal nanocompartments (Fig. 1a). HNTs comprise the low-cost[16] aluminosilicates mined from

natural deposits and are compatible with the anticorrosion coatings available on the market.[17-19] Their hollow tubular interior is suitable for the storage of ions. The pH sensing membrane wrapped around the nanocompartments is made of graphene oxide/polyamine (GO/PA). The hydroxyl groups of GO [20-27] (GO-COOH) are deprotonated at basic pH, whereas the amino groups of PA [28, 29] (PA-NH$_2$) are protonated at acidic pH. Hence, the nanoreactors assembled at a strongly acidic pH are enriched with H$^+$, whereas the nanoreactors formed at a strongly basic pH are filled with excess OH$^-$ in their interior. That is how the nanoreactors are programmed at the fabrication stage.

When immersed into a pH-neutral environment (*e.g.* into a water droplet on the aluminum alloy), the GO and PA layers acquire opposite surface charges (Fig. 1b), so that the electrostatic double-layer interaction results in a mutual attraction wrapping the nanocompartment tightly (Fig. 1a, middle). When the environmental pH balance is shifted to either acidic or basic sides (Fig. 1b), either GO or PA surface charge reduces down to zero, hence, diminishing the interlayer electrostatic attraction. This is what happens at Cu/Fe intermetallic or Al corrosion sites, see Fig. 1a, right or Fig. 1a, left, respectively. The reduced interlayer attraction allows water to enter the interlayer gap igniting the buffering reactions ($-NH_3^+ \rightleftharpoons -NH_2+H^+$ or $-COO^- +H_2O \rightleftharpoons -COOH+OH^-$) and, at the same time, loosens the wraps releasing H$^+$ or OH$^-$ ions. The released ions shift the balance of respective corrosion reactions suppressing corrosion processes.

As the layers forming the membrane carry a surface charge, the interlayer forces are governed by Coulomb interactions. The theory of electrostatic interaction of unequal double layers in an electrolyte has been developed a few decades back[30] and recently used to explain the stability of fibers made of functionalized GO/MoS$_2$ heterostructures[31]. The interlayer force can be either repulsive or attractive depending on whether the surface charge of the two neighboring layers has the same or opposite sign. The Debye screening due to the excess ions accumulated in the midgap makes the interlayer force dependent on the interlayer distance. The outcome can be presented as a diagram in Fig. 1c, which demonstrates interlayer attraction in the pH-neutral environments, as well as transition to interlayer repulsion once the pH-neutrality is upset by one of the corrosion reactions (for calculation see Supplementary Theory). The transition occurs at either about pH4 or near pH10 for the typical interlayer separations of about 1 nm. Once the nanoreactor undergoes the transition, the excess H$^+$ or OH$^-$ ions are released suppressing the respective corrosion reaction in accordance with the Le Chatelier's principle.

The corrosion protection technology includes embedding HNT/PA/GO nanoreactors into barrier sol-gel coating[32, 33]. The preparation procedure for sol-gel coating is described in the experimental part. To prepare the nanoreactors, we wrap HNT nanotubes in synthetic proton sponge[34] polyamine - 25 kDa polyethylene imine macromolecules and GO flakes (Fig. 2a). As shown in TEM images (Fig. 2b), HNT, PA and GO assemble into a wrapped structure at room temperature (RT = 25 °C). HNT forms the core, PA and GO is sequentially wrapped around HNT. The first step is to deposit a layer of PA on the outer surface of HNT. Monitoring of zeta potential vs. pH (Fig. 2d) shows that the zeta potential of the outer surface of HNT is -20 mV ~ -40 mV in the pH range between 4 and 10, while the zeta potential of PA is +60 mV ~ +20 mV in the pH range between 2 and 9. The dispersed in deionized water GO flakes have a negative zeta potential in the whole pH range. By tuning pH, we prepare the composite wraps with an adjustable number of nanolayers which can vary the zeta potential of the outmost layer to achieve compatibility of our material with different coatings. Zeta potential vs. the number of layers cycles proves the layer-by-layer wrapping (Fig. 2c). We assign the wraps as (HNT/PA/GO)$_x$, where x is the pH value ranging from 2 to 10. To reveal the composition, morphology and thermal stability of the composite wraps (Fig. 2e, f) and to optimize the ratio of HNT:PA:GO (see Supplementary Fig.1,2), we use the representative HNT/PA/GO composite prepared at pH of 4 (for details see Methods and Supplementary information).
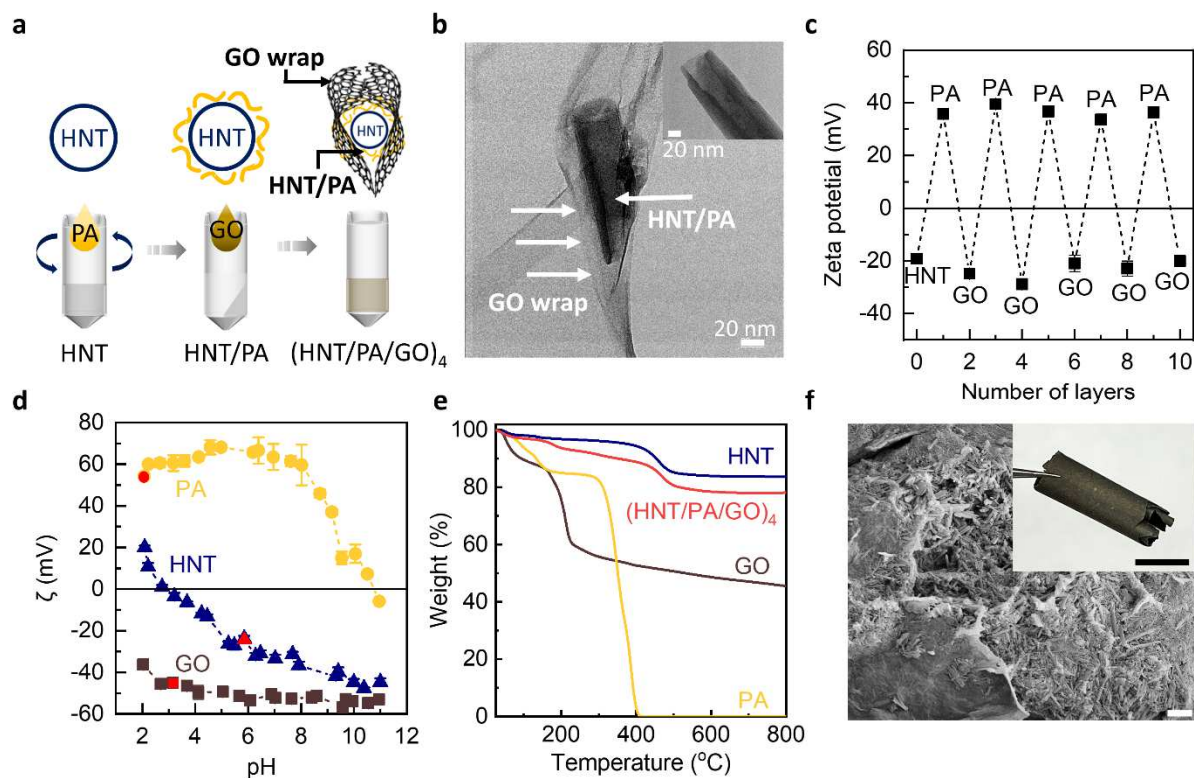
Fig. 2 Preparation and characterization of (HNT/PA/GO)₄ composites. a, A sketch of the preparation procedure of (HNT/PA/GO)₄ composites and TEM image of GO-wrapped HNT/PA nanotubes. **b,** TEM image of pure HNT, scale bar: 20 nm. **c,** Zeta potential measurements for (HNT/PA/GO)₄ composites with different numbers of layers. **d,** Zeta potential of pristine PA, GO and HNT at different pH. The pH of each component for preparing (HNT/PA/GO)₄ is marked as red (PA – pH 2, HNT – pH 6, GO – pH 3). **e,** TGA curves of HNT, PA, GO and (HNT/PA/GO)₄ composites. Heating rate: 10 °C min^{-1}, in nitrogen atmosphere. **f,** Plane view SEM image of (HNT/PA/GO)₄ powder consisting of 120 mg HNT, 12 mg PA and 6 mg GO, scale bar: 1 μm. Inset: photograph of (HNT/PA/GO)₄ solid prepared by vacuum filtration, scale bar: 1 cm.

The (HNT/PA/GO)₄ composite inherits the superior thermal stability of natural HNT nanotubes only losing 22% of weight at 800 °C (Fig. 2e). Note, that due to high thermal stability, the wraps can be used as functional fillers in existing coating technology. The Fourier-transform infrared (FT-IR) spectrum (Supplementary Fig.3) shows the characteristic peaks for HNT, PA and GO and proves (HNT/PA/GO)₄ composition. The characteristic Si-OH stretching peak and Al-OH bending peak of HNT are observed in the (HNT/PA/GO)₄ spectrum at 994 cm^{-1} and 903 cm^{-1}, respectively. In addition, the characteristic peak of the N–H group from PA appeared at 1636 cm^{-1}. The peaks at 3693 cm^{-1} and 3620 cm^{-1} are ascribed to –OH groups from hydrophilic functional groups of GO and HNT. The morphology of the wraps is revealed by AFM and SEM. Approx. 50 nm in diameter and 1–3 μm in length of HNT are observed in the AFM height map (Supplementary Fig.4a) and the SEM image (Supplementary Fig.4b). Fig. 2f shows the SEM image of the (HNT/PA/GO)₄ wraps powder prepared from aqueous dispersion (Supplementary Fig.5). We see that the wraps can be used as powder additive to the commercial top coatings and are also suitable for the formation of a continuous nanolayer for anticorrosion primer. Finally, we mix sol with HNT/PA/GO wraps to obtain the sol/HNT/PA/GO dispersion with 1:1 volume ratio(for details see Methods). After covering with the composite sol-gel coating, the surface of AA2024 became smooth and homogeneous (Supplementary Fig. 6) indicating excellent compatibility of the coating components.
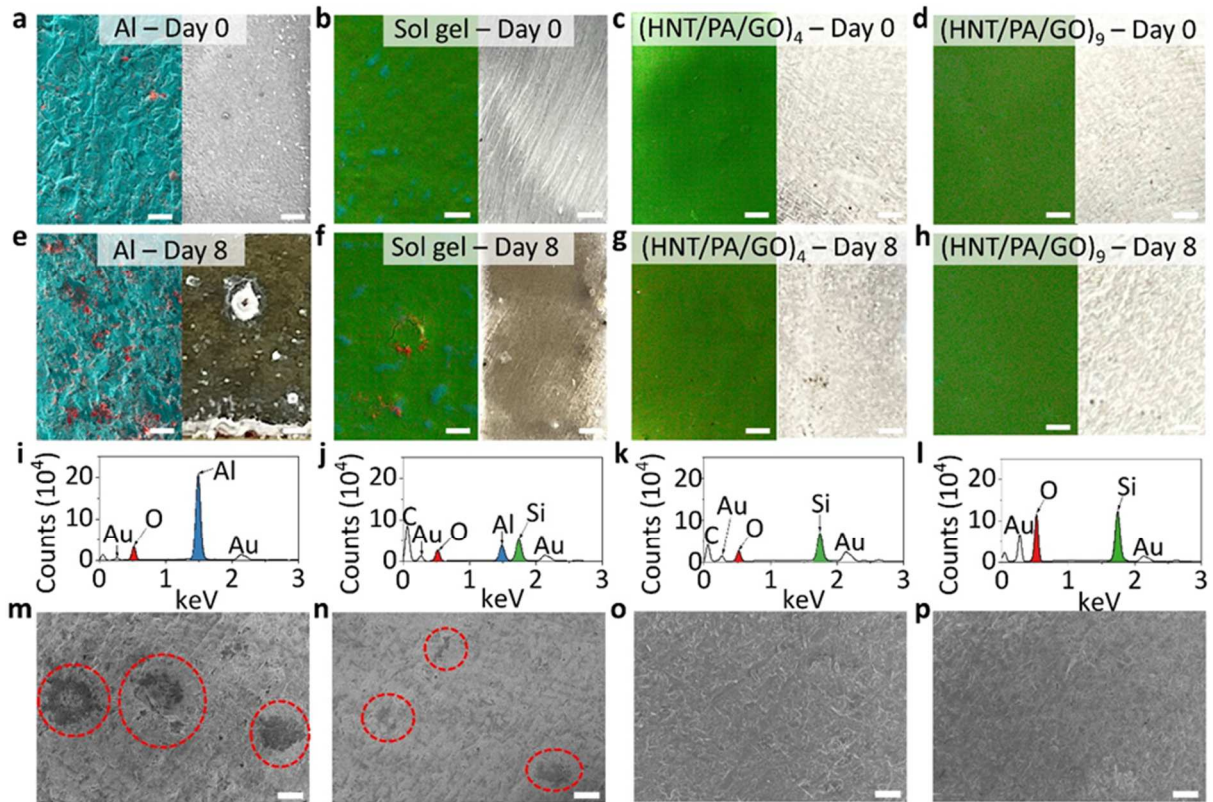
Fig. 3 Corrosion test in a saline environment. a-h, EDX mapping (left) and digital photos (right) of bare AA2024 (**a, e**), AA2024 with sol-gel coating (**b, f**), AA2024 with $(HNT/PA/GO)_4$/sol-gel coating (**c, g**) and AA2024 with $(HNT/PA/GO)_9$/sol-gel coating (**d, h**) before and after corrosion (immersed in 0.1 M NaCl for 8 days). Color of elements in EDX mapping: O – red, Al – blue, Si - green. Scale bar: EDX mapping - 20 µm; digital photos - 5 mm. **i-l,** Elemental EDX spectra of SEM images of **e-h**. **m-p,** SEM image of bare AA2024 surface (**m**), AA2024 surface after peeling off pure sol-gel coating (**n**) and AA2024 surface after peeling off $(HNT/PA/GO)_4$/sol-gel coating (**o**) or $(HNT/PA/GO)_9$/sol-gel coating (**p**) after 8-day immersion in 0.1M NaCl. Red circles indicate pitting corrosion positions on samples. Scale bar: 50 µm.

To trigger corrosion, AA2024 with nanoreactors/sol-gel coating is immersed in 0.1M NaCl for 8 days (Fig. 3). The chloride ions in the aqueous solution damage the passive oxide film due to their small radius and large penetration rate, which then cause pitting corrosion[13]. Uncovered AA2024, AA2024 with pure sol-gel coating and pristine HNT/sol-gel coating are used as references. SEM/EDX mappings show that the native AA2024 surface (Fig. 3a) and the sol-gel-covered sample (Fig. 3b) without nanoreactors are corroded after 8-day immersion. The surface of such samples is covered by the corrosion produced (Fig. 3e,f). EDX spectra show the presence of dissolved Al (Fig. 3i,j). Under coating we detect the formation of corrosion pits (Fig. 3m,n). The wraps containing composite protection coatings show an excellent corrosion protection with the surface remaining pale white and no corrosion spots are found (Fig. 3c,d,g,h). EDX spectra do not have the signals from dissolved Al (Fig.3 k,l). No corrosion pits are detected under such coatings (Fig. 3o,p). To reveal the efficiency of the nanoreactors

programmed at different pH in corrosion passivation, we monitored the anticorrosion properties of our coatings using EIS. The time response of a system perturbed by an alternating potential from EIS makes it possible to study the corrosion resistance of coatings without destruction. With the Nyquist plot of the samples after corrosion (Supplementary Fig. 7c), the equivalent circuit diagrams (Supplementary Fig. 8) are applied to fit the electrical parameters - solution resistance (Rs), coating resistance (Rc), charge transfer resistance (Rct) (Supplementary Table. 1). The performance of a coating depends on the magnitude of the impedance at low frequencies, with greater impedance standing for better protection[35]. Compared to pure sol-gel coating and HNT sol-gel coating without loading of PA and GO, and the whole range of (HNT/PA/GO)$_x$ sol-gel coatings, (HNT/PA/GO)$_4$ and (HNT/PA/GO)$_9$ sol-gel coatings show the best performance. After exposure to 0.1 M NaCl for 8 days, the impedances measured for (HNT/PA/GO)$_4$ and (HNT/PA/GO)$_9$ sol-gel coatings are at least one order of magnitude higher than those for pure sol-gel coatings and pure HNT coating (Supplementary Fig. 7a) and also exceed those for other (HNT/PA/GO)$_x$ sol-gel coatings. In the phase angle plot (Supplementary Fig. 7b), a higher angle value is recorded at a higher frequency for (HNT/PA/GO)$_4$ and (HNT/PA/GO)$_9$ sol-gel coatings, which indicates the higher stability of materials[36].

Electrochemical and electrokinetic measurements reveal that the wraps prepared at pH 4 and 9 have the most pronounced pH control capacitance and the best anticorrosion protection (Supplementary Fig. 9). The coatings prepared at pH 4 show a significant increase in both resistance and capacitance. An increase in capacitance indicates the pH control properties of the protective coating, as it increases the number of ions to form a double layer on the electrode surface. The increase in charge transfer resistance is due to the prevention of ionic charge transfer to the oxide film surface, while the buffering properties of the coating prevent any acidification caused by the hydrolysis of Al^{3+} ions. The coatings prepared at pH 9 show a significant increase in resistance since the pH control properties of the coating counteract the alkalinity that develops around the intermetallic cathodes. As expected, the coatings prepared at neutral pH do not show the pH buffering effect and the AA2024 surface is only passivated via natural oxidation mechanisms. For (HNT/PA/GO)$_7$ sol-gel coating, we observed two semicircles in the Nyquist plot. The semicircle that occurs at high frequencies stands for the resistance of the oxide film, while the other one appearing at low frequencies is the resistance at the metal surface[37].

Also, our nanomaterials provide corrosion protection and pH sensing mechanism for both the intermetallics and the metal matrix of the aluminum alloy. The pH regulation is due to the on-demand release of protons and hydroxyl ions by the nanoreactors' interior. The HNT act as nanocompartments with high buffering capacitance for the neutralization of hydroxide ions and protons. The GO/PA semipermeable membrane can sense the local pH change and adopt its permeability in response to pH shift. Anticorrosion solely relies on the natural mechanism of pH regulation of corroded surfaces and provides sustainable passivation of the corrosion process of both metal matrix and intermetallics.
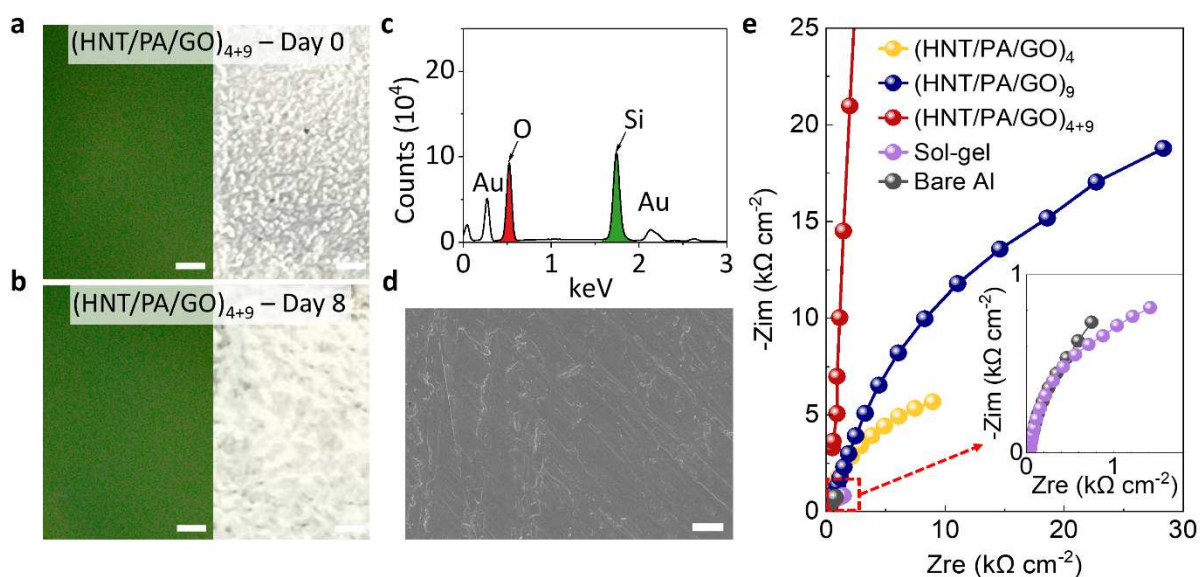

Fig. 4 Ultra-strong multi-layered self-healing (HNT/PA/GO)$_{4+9}$ coating. a-b, EDX mapping (left) and digital photos (right) of (HNT/PA/GO)$_{4+9}$ coating before (a) and after corrosion(b) when immersed in 0.1 M NaCl for 8 days. Color of elements in EDX mapping: O – red, Al – blue, Si - green. Scale bar: EDX mapping - 20 μm; digital photos - 5 mm. **c,** Elemental EDX spectra of SEM images of **b. d,** AA2024 surface after peeling off the (HNT/PA/GO)$_{4+9}$ coating after 8-day immersion in 0.1M NaCl, scale bar: 50 μm. **e,** EIS measurement of (HNT/PA/GO)$_{4+9}$ coating.

For inclusive corrosion protection and simultaneous passivation of both anodic and cathodic corrosion processes, we combine (HNT/PA/GO)$_4$ nanoreactors and (HNT/PA/GO)$_9$ nanoreactors to form an ultra-strong multi-layered coating (Supplementary Fig.10). In the integrated (HNT/PA/GO)$_{4+9}$ corrosion protection system, (HNT/PA/GO)$_9$ sol-gel coating form the top layer and (HNT/PA/GO)$_4$ sol-gel coating form the bottom layer, with an in-between insulating layer of pure sol-gel to prevent self-neutralization. The coatings with mixed nanocontainers show low efficiency (Supplementary Fig. 11). The bottom (HNT/PA/GO)$_4$ sol-gel layer targets to suppress the pitting corrosion that happens in Al matrix anode, while the

top (HNT/PA/GO)$_9$ sol-gel layer is designed to passivate the corrosion at intermetallic cathodes. Compared to (HNT/PA/GO)$_4$ and (HNT/PA/GO)$_9$ sol-gel coatings, this multi-layered (HNT/PA/GO)$_{4+9}$ sol-gel coating shows a dramatic improvement toward corrosion protection. EDX spectrum (Fig. 4 a-c) doesn't show the presence of dissolved Al after 8 days of immersion. No corrosion pits are seen in SEM images after peeling off the coating upon the 8-day-corrosion test (Fig. 4d). As measured by EIS, the resistivity on the 8th day of immersion is significantly increased by two orders of magnitude (Fig. 4e) of those for the coatings with just one type of nanoreactors. The multilayer composite coating keeps its integrity and demonstrates superior durability during corrosion test and protects the AA2024 surface from the most dangerous and usually invisible pitting corrosion.

Multicomponent materials for the future require sustainable corrosion control that is inclusive for different degradation pathways. Here we demonstrate novel eco-friendly graphene-based corrosion control nanoreactors for corrosion protection of both metal matrix and intemetalic. The nanoreactors are composed of 1D halloysite nanotubes (acting as nanocontainers) wrapped in 2D graphene oxide/polyamine (GO/PA) ion selective coating, acting as active release/adsorption membrane with sensor capabilities. Our nanoreactors can controllably release/adsorb ions (including protons) in a wide range of pH and, therefore, can ubiquitously regulate chemical processes, which is demonstrated for active corrosion protection. The novel corrosion control nanoreactors create an opportunity for preserving the life of materials and meet the goals for energy saving as well as reducing the global cost of corrosion including safety and environmental protection. Our novel anticorrosion nanoreactors are fabricated using green energy-saving technology for corrosion control with less pollution and reduced CO_2 emission. The development of novel sustainable corrosion control can lead to global savings of corrosion costs between US\$375 billion and \$875 billion annually according to Corrosion Inhibitors Market Report.[38]

Methods

Materials. Halloysite nanotubes (HNT, Sigma-Aldrich), poly(ethylene imine) (PA, branched, Mw ~25kDa, Sigma-Aldrich), aqueous graphene oxide dispersion (GO, 4 mg mL^{-1}, monolayer content > 95%, Graphenea Inc.), Polyethersulfon membrane filter (PES, 0.03 µm, 47 mm, Sterlitech Corporation), Ethanol (absolute, ≥99.8%, Sigma-Aldrich), Hydrochloric acid (HCl,), Tetraethoxysilane (TEOS,), (3-Glycidyloxypropyl)trimethoxysilane (GPTMS,), Aluminium alloy AA2024 (foil, Sigma-Aldrich, Al 93.5%/Cu 4.5%/Mg 1.5%/Mn 0.5%), with 1cm^2 surface area

exposed to the electrolyte during corrosion test. All materials were received and used without further purification.

HNT/PA/GO preparation. Aqueous GO was diluted from the original 4 mg mL^{-1} to 1 mg mL^{-1} using deionized (DI) water. While the 2 mg mL^{-1} HNT, PA dispersion was prepared by dissolving HNT or PA in DI water. HCl was added into PA dispersion to obtain the pH2 PA dispersion. 10 mL of HNT (2 mg mL^{-1}) solution and 0.1 mL of PA solution (2 mg mL^{-1}, pH2) were mixed in a 50 mL centrifuge tube. DI water was then added to the centrifuge tube to 20 mL. The HNT and PA mixture was centrifuged by Allegra X-30R Centrifuge (Beckman Coulter, 10000 RPM, 10 minutes) at room temperature. The supernatant was removed and the residual precipitation was dissolved with 20 mL of DI water. Then, the mixture was centrifuged (10000 RPM, 10 minutes) at room temperature again. The supernatant was removed and the residual precipitation is named HNT/PA. Then, 1 mL of GO dispersion (1 mg mL^{-1}) was added to obtain the final product HNT/PA/GO.

Preparation and deposition of sol-gel based HNT/PA/GO anti-corrosion coating. The sol-gel coating was prepared as the recipe described by Afsharimani et al.[39]: 11.044 mL GPTMS was mixed with 11.164 mL TEOS and 23.36 mL EtOH, and the solution was stirred for 15 minutes at room temperature. Then, 6.7 mL of 1M HCl was added drop by drop to the solution and stirred for 24 hours at 40 ºC. The resultant sol was aged for 24 h at room temperature before use. After that, HNT/PA/GO was mixed with sol in a volume ratio of 1:1 to obtain the sol/HNT/PA/GO dispersion. The coating was created by drop cast 50 µL sol/HNT/PA/GO dispersion on degreased aluminum alloy AA2024. Then, the Al plate with coating was dried for 1 hour at 120 ºC in an oven (SNOL 120/300 LSN11).

Characterization methods. Thermogravimetric analysis (TGA) was performed by TA Instrument Discovery TGA1-0247 under nitrogen at a heating rate of 10 ℃ min^{-1}. Attenuated total reflectance Fourier transform infrared (ATR-FTIR) spectra were obtained from the Bruker Alpha Platinum-ATR tool in the range of 400 – 4000 cm^{-1} with 4 cm^{-1} resolution. The scan number is 25, and the air background is subtracted during analysis. Zeta potential was measured by a MALVERN ZSU5700 Zeta Sizer. Scanning electron microscopy (SEM) images were obtained by a ZEISS Sigma 300 FE SEM system with EDX equipped. Atomic Force Microscope (AFM) measurements were conducted by AFM Bruker EQB001. The Electrochemical Impedance Spectroscopy (EIS) measurements were performed by EC-Lab® VMP-300 Potentiostat, Biologic. Scanning from 100 kHz to 0.1 Hz with Nd =6 (number of scan points per decade), and perturbation voltage of 10 mV (RMS). The platinum counter electrode and Ag/AgCl (saturated KCl) reference electrode were employed in the measurement.

Acknowledgments

Author contributions

D. V. A. and K. S. N. designed the experiments and supervised the project. K. Y., Z. H., X. L., K. N., G. K. H., N. M., performed the experiments, solved the technical issues, and checked the experimental results. TEM measurements were supported by I. V. and U. M. M. from the Center for BioImaging Science, National University of Singapore. K. Y., D. J. B., D. G. S., M.T., D. V. A., and K. S. N. co-wrote the paper. All authors discussed the results and commented on the manuscript.

Competing interests

The authors declare no competing interests.

Additional information

Supplementary information The online version contains supplementary material available.

Reference

1. Skorb, E., Shchukin, D., Mohwald, H. & Andreeva, D. Sonochemical Design of Cerium-Rich Anticorrosion Nanonetwork on Metal Surface. *Langmuir* **26**, 16973-16979 (2010).

2. Skorb, E.V. et al. Sononanoengineered magnesium-polypyrrole hybrid capsules with synergetic trigger release. *Journal of Materials Chemistry* **22**, 13841-13848 (2012).

3. Montemor, M.F. Functional and smart coatings for corrosion protection: A review of recent advances. *Surface and Coatings Technology* **258**, 17-37 (2014).

4. White, S.R. et al. Autonomic healing of polymer composites. *Nature* **409**, 794-797 (2001).

5. Andreeva, D.V., Fix, D., Möhwald, H. & Shchukin, D.G. Buffering polyelectrolyte multilayers for active corrosion protection. *Journal of Materials Chemistry* **18**, 1738-1740 (2008).

6. Montemor, M.F. Functional and smart coatings for corrosion protection: A review of recent advances. *Surf. Coat. Technol.* **258**, 17-37 (2014).

7. Twite, R.L. & Bierwagen, G.P. Review of alternatives to chromate for corrosion protection of aluminum aerospace alloys. *Prog. Org. Coat.* **33**, 91-100 (1998).

8. Bradberry, S.M., Gazzard, B. & Vale, J.A. METHEMOGLOBINEMIA CAUSED BY THE ACCIDENTAL CONTAMINATION OF DRINKING-WATER WITH SODIUM-NITRITE. *Journal of Toxicology-Clinical Toxicology* **32**, 173-178 (1994).

9. Avdeev, Y.G. & Kuznetsov, Y.I. Inhibitor protection of steel corrosion in acid solutions at high temperatures. A review. Part 2. *International Journal of Corrosion and Scale Inhibition* **9**, 867-902 (2020).

10. Long, L. et al. Comparison of MSWI fly ash from grate-type and circulating fluidized bed incinerators under landfill leachate corrosion scenarios: the long-term leaching behavior and speciation of heavy metals. *Environmental Science and Pollution Research* **29**, 15057-15067 (2022).

11. Faisal, M. et al. General properties and comparison of the corrosion inhibition efficiencies of the triazole derivatives for mild steel. *Corrosion Reviews* **36**, 507-545 (2018).

12. Market, C.I. Corrosion Inhibitors Market by Compound(Organic, Inorganic), Type(Water Based, Oil Based and VCI), Application, End-Use (Power Generation, Oil & Gas, Metal & Mining, Pulp & Paper, Utilities, Chemical), and Region - Global Forecast to 2026. (2021).

13. Yasakau, K.A., Zheludkevich, M.L. & Ferreira, M.G.S. in Encyclopedia of Interfacial Chemistry. (ed. K. Wandelt) 115-127 (Elsevier, Oxford; 2018).

14. Yasakau, K.A., Zheludkevich, M.L. & Ferreira, M.G.S. in Intermetallic Matrix Composites 425-462 (2018).

15. Lvov, Y., Price, R., Gaber, B. & Ichinose, I. Thin film nanofabrication via layer-by-layer adsorption of tubule halloysite, spherical silica, proteins and polycations. *Colloids and Surfaces a-Physicochemical and Engineering Aspects* **198**, 375-382 (2002).

16. Lvov, Y.M., Shchukin, D.G., Möhwald, H. & Price, R.R. Halloysite clay nanotubes for controlled release of protective agents. *ACS Nano* **2**, 814-820 (2008).

17. Chen, L., Yu, Z., Yin, D. & Cao, K.J.C.I. Preparation and anticorrosion properties of BTA@HNTs-GO nanocomposite smart coatings. **28**, 1-16 (2021).

18. Fix, D., Andreeva, D.V., Lvov, Y.M., Shchukin, D.G. & Möhwald, H. Application of inhibitor-loaded halloysite nanotubes in active anti-corrosive coatings. *Advanced Functional Materials* **19**, 1720-1727 (2009).

19. Borisova, D., Mohwald, H. & Shchukin, D.G. Influence of Embedded Nanocontainers on the Efficiency of Active Anticorrosive Coatings for Aluminum Alloys Part II: Influence of Nanocontainer Position. *ACS Appl. Mater. Interfaces* **5**, 80-87 (2013).

20. Yang, Z. et al. Liquid-phase exfoliated fluorographene as a two dimensional coating filler for enhanced corrosion protection performance. *Corrosion Science* **103**, 312-318 (2016).

21. Tong, Y., Bohm, S. & Song, M. The capability of graphene on improving the electrical conductivity and anti-corrosion properties of Polyurethane coatings. *Applied Surface Science* **424**, 72-81 (2017).

22. Ramezanzadeh, B., Mohamadzadeh Moghadam, M.H., Shohani, N. & Mahdavian, M. Effects of highly crystalline and conductive polyaniline/graphene oxide composites on the corrosion protection performance of a zinc-rich epoxy coating. *Chemical Engineering Journal* **320**, 363-375 (2017).

23. Qi, K., Sun, Y., Duan, H. & Guo, X. A corrosion-protective coating based on a solution-processable polymer-grafted graphene oxide nanocomposite. *Corrosion Science* **98**, 500-506 (2015).

24. Li, J. et al. Reinforcement of graphene and its derivatives on the anticorrosive properties of waterborne polyurethane coatings. *Composites Science and Technology* **129**, 30-37 (2016).

25. Hikku, G.S., Jeyasubramanian, K., Venugopal, A. & Ghosh, R. Corrosion resistance behaviour of graphene/polyvinyl alcohol nanocomposite coating for aluminium-2219 alloy. *Journal of Alloys and Compounds* **716**, 259-269 (2017).

26. Chen, C. et al. Achieving high performance corrosion and wear resistant epoxy coatings via incorporation of noncovalent functionalized graphene. *Carbon* **114**, 356-366 (2017).

27. Yang, K. et al. Electro-Thermo Controlled Water Valve Based on 2D Graphene–Cellulose Hydrogels. *Advanced Functional Materials* (2022).

28. Leng, X.Y. et al. Technology and applications of graphene oxide based membranes. *Surface Review and Letters* **28** (2021).

29. Andreeva, D.V. et al. Two-dimensional adaptive membranes with programmable water and ionic channels. *Nat. Nanotechnol.* **16**, 174-180 (2021).

30. Gregory, J. Interaction of unequal double layers at constant charge. *Journal of colloid and interface science* **51**, 44-51 (1975).

31. Tan, H. et al. Self-assembly of 2D-electrolytes into heterostructured nanofibers. *Materials Today Chemistry* **27**, 101296 (2023).

32. Koochaki, M.S. et al. The influence of the healing agent characteristics on the healing performance of epoxy coatings: Assessment of the repair process by EIS technique. *Progress in Organic Coatings* **159**, 106431 (2021).

33. Arunoday, M., Premkumar, K.P., Kumar, R. & Subasri, R. Multifunctional, environmental coatings on AA2024 by combining anodization with sol-gel process. *Ceramics International* **48**, 10969-10978 (2022).

34. Skorb, E.V., Mohwald, H. & Andreeva, D.V. How can one controllably use of natural delta pH in polyelectrolyte multilayers? *Advanced Materials Interfaces* **4** (2017).

35. del Olmo, R. et al. Hybrid sol-gel coatings applied on anodized AA2024-T3 for active corrosion protection. *Surface and Coatings Technology* **419**, 127251 (2021).

36. Sajjadi, S.A., Ahmadi, N.P. & Yazdani, S. Corrosion behavior of sol-gel coated amorphous alumina at different calcination temperatures. *Surface and Coatings Technology* **405**,

126546 (2021).

37. Hernández, H.H. et al. Electrochemical impedance spectroscopy (EIS): A review study of basic aspects of the corrosion mechanism applied to steels. *Electrochemical Impedance Spectroscopy*, 137–144 (2020).

38. Markets, M.a. Market Reports. *Markets and Markets* (2022).

39. Afsharimani, N., Duran, A., Galusek, D. & Castro, Y. Hybrid Sol-Gel Silica Coatings Containing Graphene Nanosheets for Improving the Corrosion Protection of AA2024-T3. *Nanomaterials (Basel)* **10** (2020).